Limnol. Oceanogr., 59(2), 2014, 299–310

doi:10.4319/lo.2014.59.2.0299

Oxygen photolysis in the Mauritanian upwelling: Implications for net community production

Vassilis Kitidis,[1,*] Gavin H. Tilstone,[1] Pablo Serret,[2] Timothy J. Smyth,[1] Ricardo Torres,[1] and Carol Robinson [1,a]

[1] Plymouth Marine Laboratory, Plymouth, United Kingdom
[2] Department of Ecology and Animal Biology, University of Vigo, Vigo, Spain

Abstract

We carried out 16 photochemical experiments of filtered surface water in a custom-built solar simulator and concomitant measurements of in vitro gross primary production (GPP) and respiration (R) in the Mauritanian upwelling during a Lagrangian study following three sulfur hexafluoride–labeled patches of upwelled water (P1 to P3). Oxygen photolysis rates were correlated with the absorbance of chromophoric dissolved organic matter (CDOM) at 300 nm, suggesting first-order kinetics with respect to CDOM. An exponential fit was used to calculate the apparent quantum yield (AQY) for oxygen photolysis, giving an average AQY of 0.00053 μmol O_2 (mole photons m^{-2} $s^{-1})^{-1}$ at 280 nm and slope of 0.0012 nm^{-1}. Modeled photochemical oxygen demand (POD) at the surface (3–16 mmol m^{-3} d^{-1}) occasionally exceeded R and was dominated by ultraviolet radiation (71–79%). Euphotic-layer integrated GPP decreased with time during both P-1 and P-3, whereas R remained relatively constant and POD increased during P-1 and decreased during P-3. On Day 4 of P-3, GPP and POD maxima coincided with high CDOM absorbance, suggesting "new" CDOM production. Omitting POD may lead to an underestimation of net community production (NCP), both through in vitro and geochemical methods (here by 2–22%). We propose that oxygen-based NCP estimates should be revised upward. For the Mauritanian upwelling, the POD-corrected NCP was strongly correlated with standard NCP with a slope of 1.0066 ± 0.0244 and intercept of 46.51 ± 13.15 mmol m^{-2} d^{-1}.

The world's oceans hold approximately 685 Pg of carbon (C) in the form of dissolved organic matter (DOM; Hansell and Carlson 1998). This large reservoir of C, second only in size to dissolved inorganic C, comprises a diverse range of molecules that differ in elemental composition, molecular structure, and size. Autochthonous marine DOM is thought to originate in the euphotic zone as a result of biological processes: excretion, secretion, sloppy feeding by zooplankton (Steinberg et al. 2004), and microbial processes (McCarthy et al. 1998).

The chromophoric fraction of DOM (CDOM) is involved in photochemical reactions either as a reactant and/or as a photosensitizer. These photochemical reactions lead to the decomposition of DOM with concomitant loss of CDOM absorbance and play an important role in biogeochemical cycles. (1) CDOM absorbance is typically "bleached" during exposure to ultraviolet (UV) radiation, thereby altering the spectral absorbance distribution of CDOM (Vodacek et al. 1997; Moran et al. 2000; Helms et al. 2008) and attenuation of light in the water column. (2) The preferential loss of absorbance compared to carbon (Moran et al. 2000; Vähätalo and Wetzel 2004) and concomitant decrease in aromaticity (Stubbins et al. 2010) and molecular weight (Helms et al. 2008) show that photochemical reactions alter the composition of DOM. (3) Photochemical reactions involving DOM produce climatically active trace gases (e.g., CO_2, CO; Mopper et al. 1991; Miller and Zepp 1995), nutrients (e.g., NH_3; Bushaw et al. 1996; Kitidis et al. 2006*b*), and low-molecular-weight organic compounds (Kieber et al. 1989).

Dissolved, molecular oxygen (O_2) acts as a major oxidant in photochemical reactions involving CDOM, resulting in apparent O_2 consumption (Laane et al. 1985). Photochemical activation or reduction of O_2 gives rise to reactive oxygen species (ROS) including short-lived hydroxyl (OH), singlet oxygen ($^1O_2$), and superoxide ion (O_2^-) radicals as well as relatively longer-lived hydrogen peroxide (H_2O_2; Zafiriou 1974; Zepp et al. 1992; Micinski et al. 1993). In turn, ROS play a crucial role in the photochemical decomposition of DOM (Scully et al. 2003), trace metal redox cycling (Rose and Waite 2006), and may inhibit biological processes (Kaiser and Sulzberger 2004). The wavelength dependence of these reactions typically decreases with increasing wavelength from ultraviolet B (UVB) to visible radiation for O_2 (Andrews et al. 2000), $^1O_2$ (Zepp et al. 1977), and H_2O_2 (O'Sullivan et al. 2005).

Different methods are currently used for the determination of oxygen-based gross primary production (GPP), respiration (R), and net community production (NCP) in marine plankton communities. These fall broadly into two categories: in vitro incubation methods and geochemical methods. During in vitro light–dark incubations where the production–consumption of oxygen is measured over time (typically 24 h), samples are placed in borosilicate glass bottles and exposed to sunlight, either on deck or in situ (Robinson et al. 2009). Since associated light-filters shield

* Corresponding author: vak@pml.ac.uk

[a] Present address: School of Environmental Sciences, University of East Anglia, Norwich, United Kingdom

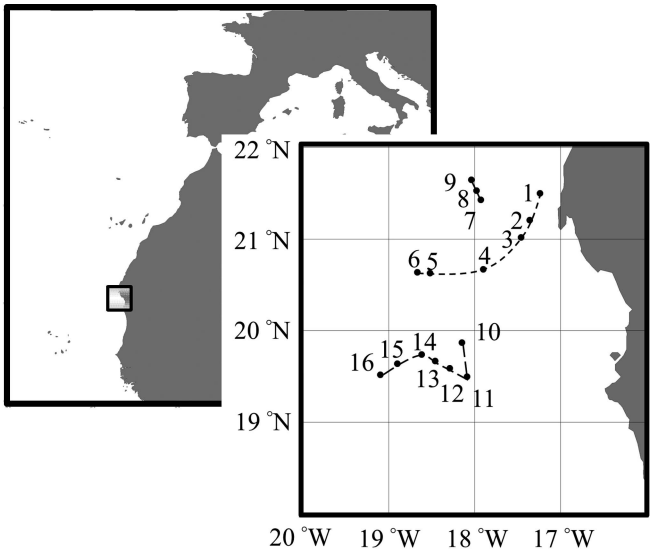

Fig. 1. Study area and station locations. Dashed line follows the first ^{3}He and SF_6–labeled patch of upwelled water (P-1, Sta. 1–6), solid line follows the second patch (P-2, Sta. 7–9), and log-dash line follows the third patch P-3, Sta. 10–16). Figure created with Ocean Data View (R. Schlitzer, Ocean Data View, http://odv.awi.de, 2013).

the samples from UV radiation, photochemical reactions are thought to be largely inhibited. The measured changes in O_2 are therefore attributed to biological processes. Three different geochemical approaches are used for the determination of plankton NCP. (1) By examining the evolution of O_2 during high-frequency profiles in the euphotic layer (Sambrotto and Langdon 1994). (2) Measurements of O_2 : Ar ratios (Kaiser et al. 2005). Ar, being inert, is controlled by air–sea exchange, whereas O_2 is controlled by air–sea exchange and biological processes. (3) NCP is estimated from differences in the isotopic composition of O_2 ($^{16}O_2$, $^{17}O_2$, and $^{18}O_2$) between air and seawater (Luz and Barkan 2000). These geochemical methods assume that any changes in O_2 concentration, O_2 : Ar, or O_2 isotopic composition are due to NCP, after corrections for sea–air exchange of O_2. However, they do not account for photochemical oxygen consumption and may therefore underestimate NCP.

Under climate projections for the 21st century, stratification of the surface ocean is predicted to increase (Bopp et al. 2001). This could increase the residence time of DOM in the euphotic zone, potentially enhancing the role of photochemical reactions in biogeochemical cycles. Though much of our understanding of these processes is derived from fresh- or estuarine waters, previous studies have observed photochemical O_2 consumption in the North Sea (Laane et al. 1985), Adriatic (Obernosterer and Herndl 2000), subtropical Atlantic (Obernosterer et al. 2001), and Gulf of Mexico (Andrews et al. 2000). In one study, photochemical oxygen demand (POD) was found to exceed microbial respiration in open-ocean waters of the subtropical Atlantic (Obernosterer et al. 2001). Similarly, Laane et al. (1985) found that POD could consume 5–40% of photosynthetically produced O_2. POD may thus represent a substantial sink for dissolved O_2 in clear marine waters that is currently unaccounted for. In this study, we investigated photochemical O_2 demand during three Lagrangian experiments in a Mauritanian upwelling filament and test the hypothesis that POD is a substantial sink for O_2 in the euphotic layer.

Methods

Study area and sampling—Our experiments were carried out onboard the Royal Research Ship *Discovery*, during cruise D338 in the Mauritanian upwelling (15 April to 29 May 2009; Fig. 1). The objective of the cruise was to study the biogeochemistry of an upwelling filament by following patches of recently upwelled, dual tracer–labeled (^{3}He and SF_6) water, offshore. Three not overlapping patches (initial size 4 × 4 km) were deployed on 22 April, 08 May, and 15 May 2009, hereafter P-1, P-2, and P-3, respectively. In addition to the ^{3}He and SF_6 label, each patch was marked by one central and four peripheral drifters. Briefly, the patch center was identified daily by overnight mapping of SF_6 concentration, determined by gas chromatography. The ship was then positioned at the center of the patch for a predawn station. Though the initial objective was to label one patch and follow it for the duration of the cruise, P-1 was abandoned as it grew to a size that we were unable to survey after 8 d, P-2 subducted after 3 d, and finally P-3 was followed for 8 d.

Sampling and irradiation setup—In situ temperature and salinity were recorded from a conductivity–temperature–depth sensor (SBE 911plus/917plus, Seabird) mounted on a 24 × 20 liter bottle hydrocast. Chlorophyll *a* was measured with a fluorometer (model Aquatracka, Chelsea Instruments) mounted on the hydrocast. The fluorometer was calibrated fluorometrically following acetone extraction (Welshmeyer 1994). Irradiance was measured with a UV (model Ramses-ACC-UV, TriOS) and photosynthetically active radiation (PAR) sensor (SKE 510, Skye Instruments). Underwater irradiance ($Ed_{\lambda,z}$) was determined at four UV wavelengths (305, 325, 340, and 380 nm) using a Satlantic UV-507 radiometer and a PAR sensor (model 0046-3097, Chelsea Instruments) attached to an optical profiling rig. Light attenuation coefficients at these wavelengths (Kd_λ), were determined by the slope of $\ln(Ed_{\lambda,z})$ against depth between the surface and the spectrally varying 1% irradiance level using the upcast part of the vertical profile. This was done by median binning of the Ed_λ profile into 2 m depth intervals from a depth of 1 m and below and then carrying out the regression. Only profiles where $R^2 > 0.98$ for the Kd_λ regression were selected for further analysis. This strict criterion was set to automatically and objectively remove vertical profiles where there were strong vertical inhomogeneities or remaining surface irradiance changes.

Water for 16 irradiation experiments was collected from the predawn hydrocast in a 20 liter glass vessel cleaned with dilute HCl. All samples were collected from the sea surface. Each sample was immediately gravity filtered into a second 20 liter, acid-cleaned glass vessel, through sequential 0.2 μm and 0.1 μm AkroPak 1000 filters. Both 20 liter vessels were housed

in wooden crates to avoid light exposure of the sample. Microbial counts of the filtrate by flow cytometry were $< 10^3$ cells mL^{-1}, $< 1\%$ of the ambient unfiltered counts. The filtered sample was used to fill 8–12 quartz and 8–12 borosilicate glass stoppered bottles (nominal volume 125 mL) using clean silicon tubing. The tubing was placed at the bottom of each bottle and the water allowed to overfill with 3× the volume of the bottle. Quartz bottles were irradiated (*see* below), while borosilicate bottles were used to determine the initial concentration of O_2 and as dark controls (wrapped in double aluminum foil). A separate test showed that O_2 concentration determined in quartz or borosilicate bottles did not differ when filled with the same sample (*t*-test, $t = 1.84$, degrees of freedom [df] = 7, $p > 0.05$). Additional samples for CDOM absorbance were irradiated in custom-made 1 liter quartz flasks (57 mm diameter; Kitidis et al. 2011).

For our irradiation experiments, we used the setup described by Kitidis et al. (2011). Irradiated quartz bottles and 1 liter flasks were placed horizontally in a custom-built solar simulator fitted with UV400W (Commercial Lamp Suppliers) and 150 W metal halide (model MHN-TD, Phillips) lamps (Kitidis et al. 2011). The bottles and flasks were submerged in running seawater for cooling, while the bottom and sides of the irradiation tray were painted black to minimize reflectance. Irradiance in our solar simulator was as follows: 4.4 W m^{-2} UVB (290–320 nm), 49.1 W m^{-2} ultraviolet A (UVA; 320–400 nm), and 159.1 W m^{-2} PAR (400–800 nm). This was in good agreement for ambient UVA and UVB at noon, but underestimated PAR by 50–65% in our study area (Kitidis et al. 2011). For selected experiments, replicate samples were placed in a second identical solar simulator fitted with a long-pass Perspex sheet to block UV radiation (cutoff 390 nm). Dark control samples were also placed in the incubators. Each treatment (initial concentration, UV+visible, visible-only, and dark control) was replicated 4–6 times for O_2 and 2–3 times for CDOM absorbance. Samples were irradiated for 19.3–24.8 h.

Gross production and R incubations—Additional incubations were carried out on deck for the determination of GPP, net primary production, and R (Serret et al. 2001; Gist et al. 2009). Samples were collected predawn from six depths in 10 liter acid-cleaned carboys (wrapped in black plastic bags to minimize light exposure). Sampling depths corresponded to the 97%, 55%, 33%, 14%, 3%, and 1% light depths. The only exception to this sampling was on 24 April 2009, when samples were only collected from two depths corresponding to the 97% and 55% light levels. Each carboy was subsampled into 12 × 125 mL glass stoppered bottles that were divided into three treatments: (1) Start (fixed immediately), (2) Light (placed in on-deck incubators for 24 h), and (3) Dark (wrapped in double aluminum foil and placed in on-deck incubators for 24 h). The on-deck incubators were cooled by continuously flowing surface seawater from the ship's underway supply and fitted with UV-opaque neutral-density light filters to approximate the ambient light field. The "Start" subset of samples was kept in the dark, submerged in water, until analysis on the following day along with the corresponding "Light" and "Dark" sample subsets. The concentration of O_2 was determined in all samples (*see* below for analytical details). GPP was calculated as the difference between Light and Dark samples. R was calculated as the difference between Dark and Start samples, and NCP was calculated as the difference between Light and Start samples.

Analytical methods—The concentration of O_2 was determined by automated Winkler titration (Carritt and Carpenter 1966). Briefly, O_2 is precipitated with alkaline iodide (NaOH + NaI) and $MnSO_4$ and the samples stored in a water bath at room temperature until analysis (< 36 h). The precipitate is dissolved by addition of H_2SO_4 and titrated against thiosulfate (transmission endpoint detection). The thiosulfate was calibrated every 2–3 d against 0.1 mol L^{-1} KIO_3 standards (34273, Sigma-Aldrich). O_2 saturation with respect to atmospheric equilibrium was calculated from the solubility of O_2 at in situ temperature, salinity, and pressure (Benson and Krause 1984; Garcia and Gordon 1992).

CDOM absorbance was measured spectrophotometrically (model Lambda 35, Perkin Elmer) using 10 cm cells and referenced against Milli-Q water. Absorbance data between 250 nm and 800 nm were offset corrected for instrument drift by subtracting the average absorbance in the 680–700 nm range (Kitidis et al. 2006*a*). The CDOM absorption coefficient (α_λ) was calculated from:

$$\alpha_\lambda = 2.303 \times A_\lambda / d \quad (1)$$

where d is the cell pathlength (0.1 m) and A_λ is the absorbance of the sample. The α_λ data were fitted with a nonlinear exponential fit and a linear fit to ln-transformed data:

$$\alpha_\lambda = \alpha_{\lambda 0} \times e^{-S \times (\lambda - \lambda 0)} \quad (2)$$

where S is the spectral slope calculated over the 290–350 nm ($S_{290–350}$) and 250–650 nm ($S_{250–650}$) ranges for the nonlinear model and 275–295 nm ($S_{275–295}$) and 350–400 nm ($S_{350–400}$) for the ln-transformed linear model. These wavelength ranges were chosen as their values convey information about the origin of DOM, its radiation exposure history, and molecular weight (Kitidis et al. 2006*a*; Helms et al. 2008). Specifically, the slope ratio S_R ($S_{275–295} : S_{350–400}$) has been shown to be related to DOM molecular weight (Helms et al. 2008). Similarly, $S_{290–350}$ and $S_{250–650}$ may be used to identify sample provenance and photochemical transformations (Kitidis et al. 2006*a*).

Photochemical rate calculations—Photochemical oxygen demand rates were calculated from the concentration difference between light (UV+visible or visible only) and dark treatments. O_2 concentration in dark bottles was indistinguishable from the start of the experiments (*t*-test, $t = 0.5$ to 1.5, df = 5 to 10 depending on number of replicates, $p > 0.05$). Photochemical O_2 consumption rates ($\partial[O_2]/\partial t$) can be modeled according to Eq. 3 (Miller et al. 2002):

$$\partial[O_2]/\partial t = \int I_\lambda \times A / V^* \times \left(1 - e^{\alpha\lambda \times 1}\right) \times (AQY_{O2,\lambda}) \times \partial\lambda \quad (3)$$

where I_λ is the irradiance at wavelength λ (units: mol photons m^{-2} h^{-1} nm^{-1}), A is the horizontal surface area of the irradiation flasks (2.94×10^{-3} m^2), V* is the volume of the flasks (0.087 liters) adjusted for refraction using the Fresnel equations (Kitidis et al. 2011), α_λ is the CDOM absorption coefficient at wavelength λ, and l is the flask path length (0.031 m). $AQYO_{2,\lambda}$ is the apparent quantum yield (AQY) of the reaction, in this case the number of mol O_2 consumed per mol photons absorbed at wavelength λ. All of the parameters in Eq. 3 are known with the exception of $AQY_{O2,\lambda}$. We therefore applied an iterative mathematical optimization, so that the model ratios of UV+visible : UV-only and the magnitude of photoconsumption rates were equal to the respective experimental ratios and rates. The formula used to fit $AQYO_{2,\lambda}$ followed an exponential decrease with increasing wavelength:

$$AQY_{O2,\lambda} = AQY_{O2,\lambda 0} \times e^{-S_{AQY} \times (\lambda - \lambda 0)} \quad (4)$$

where $AQYO_{2,\lambda 0}$ is the $AQYO_{2,\lambda}$ at wavelength $\lambda 0$ (280 nm) and S_{AQY} is the slope of the exponential decrease. The latter is determined by iterative model calculations matching the model rate ratio of UV+visible : UV-only rates to observations, while $AQYO_{2,\lambda 0}$ can be determined iteratively from the UV+visible rate once S_{AQY} is known. Although the technique has been widely applied to other photochemical reactions (Vähätalo and Zepp 2005; Stedmon et al. 2007), it rests on the underlying assumption that the $AQYO_{2,\lambda}$ follows this exponential model. The limitations of this are discussed in detail later in this paper (*see* Discussion).

Photochemical model—We used our experimental results to parameterize a simple one-dimensional photochemical model coded in R (http://www.r-project.org/). The model consists of 29 discrete depth layers of variable thickness, increasing with depth from 0.1 m thickness at the surface to 10 m thickness for the 50–60 m layer (Kitidis et al. 2011). The upper (surface) and lower (60 m depth) boundaries of the water column are open to gas exchange and diffusive exchange with deep waters, respectively. GPP at depth Z (GPP_Z) was parameterized by fitting a photosynthesis–irradiance model (Platt et al. 1980) to measured GPP data (normalized by in situ Chl *a* concentration) against integrated irradiance in each respective incubator.

$$GPP_Z = P^B_{max} \times \left(1 - e^{\left(-\alpha B \times I_Z / P^B_{max}\right)}\right) \quad (5)$$

where P^B_{max} is the maximum Chl *a*–normalized GPP rate (mean of measured at 97% and 55% light), αB is the light-limited slope, and I_Z is the PAR irradiance at depth Z. R was calculated as the mean respiration from six depths for each corresponding profile. POD was described as a function of scalar irradiance ($I_{\lambda,Z}$), $AQYO_{2,\lambda}$, and CDOM absorbance (α_λ) at wavelength λ (Miller et al. 2002):

$$POD = \int I_{\lambda,Z} \times AQY_{O2,\lambda} \times \alpha_\lambda \quad (6)$$

The integration is carried out for the UVA, UVB, and PAR spectral bands. Light attenuation in the water column was described by Lambeert–Beer's law using the measured light attenuation coefficient, $K_{d,\lambda}$ (Smyth 2011):

$$I_{\lambda,Z} = I_{\lambda,0} \times e^{-K_{d,\lambda} \times Z} \quad (7)$$

where $K_{d,\lambda}$ is the light attenuation coefficient at 310, 350, and 450 nm for UVB, UVA, and PAR, respectively. These wavelengths were selected as representative of UVB, UVA, and PAR, respectively, and were calculated from the exponential fit of K_d vs. wavelength for the readings at 305, 325, 340, and 380 nm. $I_{\lambda,Z}$ and $I_{\lambda,0}$ are the scalar irradiance at wavelength λ, at depth Z and the surface, respectively. Scalar irradiance at the surface was calculated from measured spectral irradiance ($I_{\lambda,solar,0}$) and corrected for refraction (Miller et al. 2002):

$$I_{\lambda,0} = I_{\lambda,solar,0}/\mu \quad (8)$$

where μ is the average near-surface cosine:

$$1/\mu = F_{dir,\lambda}/\cos\theta \times 1.19 \times F_{diff,\lambda} \quad (9)$$

where $F_{dir,\lambda}$ and $F_{diff,\lambda}$ are the direct and diffuse fractions of $I_{\lambda,solar,0}$. The direct and diffuse fractions of spectral irradiance were calculated with the SolRad 1.2 program (Pelletier 2008) using the Bird and Hulstrom model (Bird and Hulstrom 1981).

Surface spectral irradiance (integrated over the UVB, UVA, and PAR ranges), the respective light attenuation coefficients ($K_{d,\lambda}$), AQY ($AQY_{O2,UVB}$, $AQY_{O2,UVA}$, and $AQY_{O2,vis}$), and CDOM absorption coefficients (α_{UVB}, α_{UVA}, and α_{vis}) were determined as above and used as input parameters for the model.

Results

CDOM properties and photodegradation—Table 1 shows the initial CDOM absorbance properties for all our experiments. The highest α_{300} was found relatively close inshore prior to the deployment of P-1. Initial α_{300} for our experiments was generally lower in the northern patch (P-1) compared to the southern patch and showed a small decrease between the start and end of the period during which the patch was followed (P-1: 0.56 m^{-1} and 0.49 m^{-1} at the start and end, respectively; P-2: 0.57 m^{-1} and 0.55 m^{-1}, respectively; P-3: 0.61 m^{-1} and 0.54 m^{-1}, respectively). Nevertheless, a maximum of 1.24 m^{-1} was observed during Day 4 of P-3.

$S_{275–295}$, $S_{290–350}$, and $S_{250–650}$ slope values were in the range of 0.0047–0.0327 nm^{-1}, 0.0169–0.0238 nm^{-1}, and 0.0161–0.0227 nm^{-1}, respectively. Initial S_R values for our samples were in the range of 0.28–2.24. Out of 16 experiments, 14 had initial S_R values > 1.73 (up to 2.24), while a further three (numbers 1, 7, and 13) had S_R values in the range of 0.28–0.67. Loss of CDOM absorbance was observed during all irradiation experiments, whereas dark control samples did not change substantially. The loss of CDOM absorbance was most pronounced in the UV region of the spectrum, specifically around 270 nm for the 14 experiments with SR values > 1.73. For the three samples with S_R values < 1, the highest CDOM absorbance loss was red-shifted, centered around 295 nm (Fig. 2). The latter

Table 1. Sampling details and initial CDOM properties for irradiated waters. Patch, Day refers to ^{3}He and SF_6 patch number, and day within each patch (Day −1 refers to the day of sampling before ^{3}He and SF_6 deployment).

Expt	Date (2009)	Latitude (°N)	Longitude (°W)	Patch, Day	α_{300} (m^{-1})	α_{350} (m^{-1})	$S_{275–295}$ (nm^{-1})	S_R	$S_{290-350}$ (nm^{-1})	$S_{250–650}$ (nm^{-1})
1	21 Apr	21.5	17.24	P1, −1	1.32	0.29	0.0047	0.28	0.0169	0.0161
2	23 Apr	21.21	17.36	P1, 1	0.56	0.26	0.0275	1.55	0.0219	0.0208
3	24 Apr	21.02	17.46	P1, 2	0.47	0.19	0.0293	1.89	0.0238	0.0227
4	27 Apr	20.67	17.9	P1, 5	0.55	0.24	0.0269	1.73	0.0218	0.0205
5	29 Apr	20.63	18.52	P1, 7	0.51	0.21	0.0280	2.20	0.0218	0.0205
6	30 Apr	20.64	18.67	P1, 8	0.49	0.19	0.0292	1.82	0.0229	0.0215
7	08 May	21.43	17.93	P2, −1	1.05	0.26	0.0099	0.62	0.0187	0.0176
8	09 May	21.53	17.98	P2, 1	0.57	0.23	0.0267	1.79	0.0216	0.0207
9	10 May	21.65	18.04	P2, 2	0.55	0.24	0.0278	1.88	0.0221	0.0210
10	14 May	19.87	18.15	P3, 1	0.61	0.25	0.0327	2.24	0.0230	0.0213
11	16 May	19.5	18.09	P3, 2	0.51	0.18	0.0289	1.90	0.0236	0.0223
12	17 May	19.59	18.29	P3, 3	0.51	0.19	0.0286	1.84	0.0231	0.0218
13	18 May	19.67	18.46	P3, 4	1.24	0.35	0.0101	0.67	0.0176	0.0164
14	19 May	19.74	18.62	P3, 5	0.72	0.33	0.0232	2.19	0.0194	0.0179
15	21 May	19.64	18.9	P3, 7	0.68	0.27	0.0256	2.01	0.0213	0.0198
16	22 May	19.52	19.1	P3, 8	0.54	0.22	0.0282	1.85	0.0226	0.0213

samples showed a mycosporine-like amino acid (MAA) absorbance shoulder prior to irradiation (e.g., experiment [expt] 13 in Fig. 2). This MAA absorbance shoulder was completely photodegraded during the course of the corresponding experiments. Irradiation caused an increase in the value of the CDOM spectral slopes, $S_{275–295}$, $S_{290–350}$, and $S_{250–650}$, in all of our experiments, with the biggest change in slope in the three experiments with MAA absorbance characteristics.

POD and AQYs—Photochemical O_2 consumption was observed in all of our experiments. Full-spectrum POD from our experiments was in the range of 19–79 nmol L^{-1} h^{-1} and 0–61 nmol L^{-1} h^{-1} under the visible-only spectrum (Table 2). For visible-only treated samples, we found consistently lower POD rates compared to the corresponding full-spectrum samples. The highest rates were found in the three experiments where the CDOM spectra showed MAA absorbance characteristics. The full-spectrum POD was significantly correlated with CDOM absorbance at 300 nm ($R^2 = 0.483$, $n = 15$, $p < 0.05$; POD $= 48.6 \times \alpha_{300} + 7.7$). However, no significant correlation was found between POD rates and α_{350}. The mean full-spectrum POD rate was significantly different from the mean visible-only rate (paired t-test, $t = 5.6$, df $= 7$, $p < 0.001$). The full-spectrum and UV-only rates were strongly correlated (Spearman $R^2 = 0.98$, $p < 0.01$, $n = 8$), with a slope of 0.80, suggesting that UV radiation in our incubators was responsible for 80% of the observed POD (Fig. 3). Therefore, in order to derive the slope of the POD AQY for experiments where we did not have data under the visible-only treatment (*see* Table 2), we applied a ratio of 1 : 4 (visible : UV) to calculate corresponding UV rates. Propagating the error of oxygen photolysis rates through the calculations for the AQY parameters resulted in small errors (< 2%) for the AQY at 350 nm (AQY_{350}), but relatively large errors for S_{AQY} (error range: 27–37%; Table 2). The corresponding visible : UV ratio varied between 1 : 3 and 1 : 5. The AQY for photochemical oxygen consumption at 350 nm (AQY_{350}) was in the range of 1.10–8.67 $\times$ 10^{-4} mol O_2 (mole photons m^{-2} $s^{-1})^{-1}$ and remained relatively constant during P-1, but showed a decreasing trend with time during P-3 (Table 2).

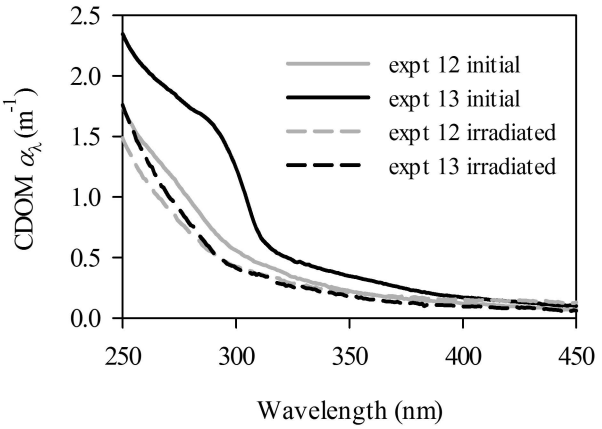

Fig. 2. Initial and irradiated CDOM absorption spectra experiments (expts) 12 and 13. Expt 13 was characterized by a mycosporine-like amino acid (MAA) absorbance shoulder.

GPP, R, and NCP—Surface Chl *a* was in the range of 0.1–9.0 μg m^{-3}, with the highest values recorded inshore, close to the source of upwelling. Surface GPP and R were in the range of 6.4 ± 0.6 to 52.5 ± 2.6 μmol L^{-1} h^{-1} and 2.8 ± 0.6 to 7.4 ± 1.4 μmol L^{-1} h^{-1}, respectively. GPP was generally constant in the uppermost 15–20 m and then decreased with depth, whereas R remained relatively constant throughout the euphotic zone. Depth-integrated (over the euphotic zone; surface to 1% light depth), daily NCP (NCP_{int}) was positive throughout P-1 (126–1328 mmol O_2 m^{-2} d^{-1}) and P-3 (139–889 mmol O_2 m^{-2} d^{-1}), suggesting net autotrophy. Euphotic-layer depth-integrated GPP (GPP_{int}) and NCP_{int} followed a decreasing trend with time for both patches, with a maximum in the early stages of the Lagrangian experiments (Day 2 for P-1 and Day 4 for

Table 2. Photochemical oxygen demand (POD; units: nmol L^{-1} h^{-1}) rates under full-spectrum, visible-only, and UV-only irradiations (± standard error [SE]). Calculated AQY for POD at 350 nm (units: $\times 10^{-4}$ mol O_2 [mole photons m^{-2} s^{-1}]$^{-1}$) and AQY slope (units: $\times$ 10^{-2} nm^{-1}, ± SE propagated from POD rates).

Expt	Patch, Day	POD	POD—visible	POD—UV	$AQYO_{2,\ 350}$	AQY slope
1 (MAA)	P1, −1	79±5			3.45±0.01	0.99±0.33
2	P1, 1	48±5	10±3	39±5	2.82±0.04	1.12±0.39
3	P1, 2	41±4			3.10±0.03	1.13±0.39
4	P1, 5	44±9			2.65±0.04	1.24±0.36
5	P1, 7	50±8			3.22±0.03	1.35±0.37
6	P1, 8	32±6	5±10	27±12	2.39±0.003	1.07±0.38
7 (MAA)	P2, −1	74±7	16±3	59±8	3.62±0.02	1.07±0.34
8	P2, 1	37±7			2.25±0.02	1.18±0.38
9	P2, 2	19±1	2±3	17±3	1.14±0.01	1.22±0.38
10	P3, 1	37±6	9±6	27±8	2.07±0.02	1.27±0.35
11	P3, 2	48±5			3.62±0.02	1.10±0.40
12	P3, 3	23±4	1±4	23±5	1.74±0.01	1.07±0.39
13 (MAA)	P3, 4	59±9			2.21±0.01	1.22±0.34
14	P3, 5	27±5	6±4	22±6	1.13±0.01	1.59±0.37
15	P3, 7	18±7	3±6	14±9	0.89±0.01	1.35±0.37
16	P3, 8	14±10			0.89±0.01	1.20±0.37

P-3). Euphotic-layer depth-integrated R (R_{int}) remained relatively constant during both P-1 and P-3 and increased as a proportion of GPP_{int}, from 24% to 59% and 40% to 68%, respectively.

Model results—Figure 4 shows a typical example of measured and modeled GPP and R and the corresponding P-I curve for 27 April 2009 (Day 5 in P-1). The model was generally in good agreement with observations, both for GPP and R. Note that all model results are preceded by the prefix "m."

Euphotic-layer depth-integrated $mGPP_{int}$, mR_{int}, and $mPOD_{int}$ from our model were in the range of 272–1480 mmol O_2 m^{-2} d^{-1}, 106–340 mmol O_2 m^{-2} d^{-1}, and 13–97 mmol O_2 m^{-2} d^{-1}, respectively (Fig. 5). $mNCP_{int}$ was in the range of 88–1217 mmol O_2 m^{-2} d^{-1} for P-1 and 140–889 mmol O_2 m^{-2} d^{-1} for P-3. $mNCP_{int}$ was strongly correlated with measured NCP_{int} (Spearman $R^2 = 0.94$, $p < 0.0001$, $n = 11$), with a slope of 0.89 ± 0.07 and intercept indistinguishable from zero (−15 ± 46 mmol O_2 m^{-2} d^{-1}).

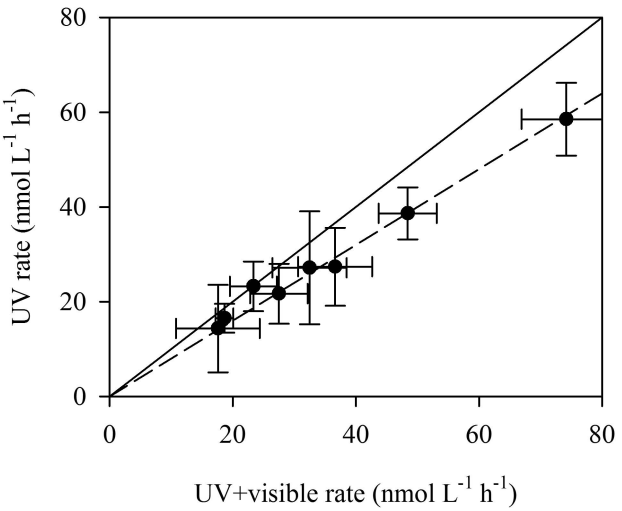

Fig. 3. UV+visible vs. UV-only POD rate. The solid line represents a 1 : 1 relationship. Dashed line represents a UV : visible rate ratio of 1 : 4.

Surface mPOD rates were in the range of 3.0–15.7 μmol L^{-1} d^{-1}. Depth-integrated $mPOD_{int}$ followed a generally increasing trend with time during P-1 (range: 33–97 mmol O_2 m^{-2} d^{-1}) and a decreasing trend during P-3 (range: 13–77 mmol O_2 m^{-2} d^{-1}), with the exception of a pronounced maximum on Day 4 (Fig. 5). The latter coincided with maxima in CDOM absorbance at 300 nm and GPP_{int} (as well as $mGPP_{int}$). The AQY_{350} values were also higher than on the previous or the following day, deviating from a decreasing trend with time. The corresponding CDOM spectrum revealed a clear MAA-like shoulder (expt 13 in Tables 1 and 2; spectrum in Fig. 2). UVA radiation accounted for 39–65% of $mPOD_{int}$ during P-1, and 36–43% during P-3 (Fig. 5B). However, the contribution of UVA only dominated on the first day of P-1 (23 April 2009) and was otherwise comparable to P-3. UVB radiation accounted for only a small fraction of the total rate (1–2%). The majority of mPOD in the water column was therefore accounted for by irradiance in the visible range of the spectrum. $mPOD_{int}$ varied between 3% and 36% of $mGPP_{int}$ and 4% and 59% of mR_{int}, suggesting that photochemical oxygen consumption may be a substantial sink for O_2 in surface waters. The proportion of POD relative to $mGPP_{int}$, increased with decreasing $mNCP_{int}$, reaching its highest values as the ecosystem was approaching a net trophic balance ($mNCP_{int} \sim 0$; i.e., autotrophy equal to heterotrophy).

Discussion

CDOM photobleaching and POD—The initial spectral properties of our samples (α_{300}, α_{350}, $S_{290-350}$, and $S_{250-650}$) fall within the range of values described by previous studies in the Atlantic Ocean (Nelson et al. 1998; Kitidis et al. 2006*a*). Based on the initial S_R values of our samples and according to the relationship found by Helms et al. (2008),

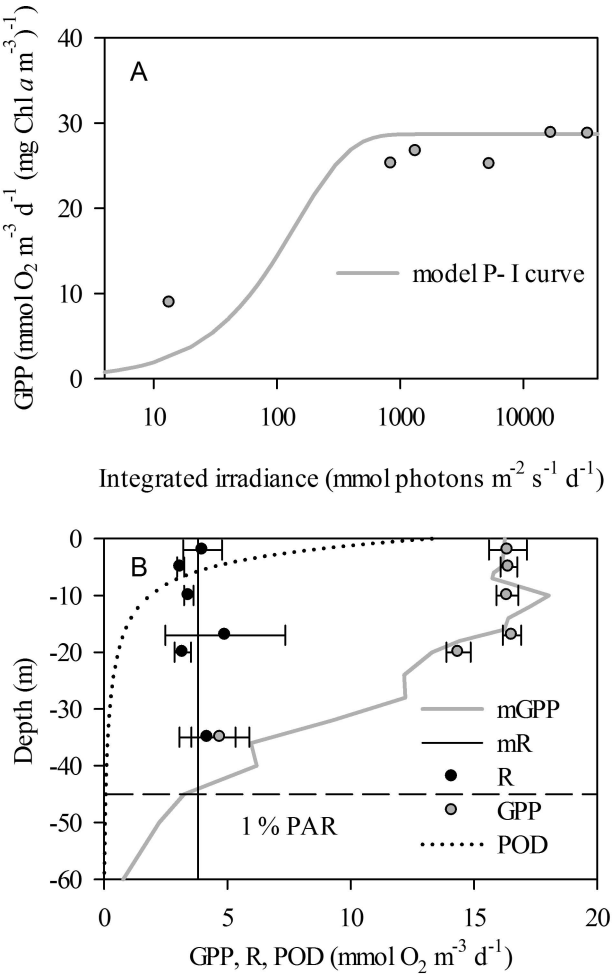

Fig. 4. (A) Typical example of data and modeled P-I curve and (B) measured and modeled GPP, R, and POD from 27 April 2009 (Day 5 in P-1). All model results are preceded by the prefix "m."

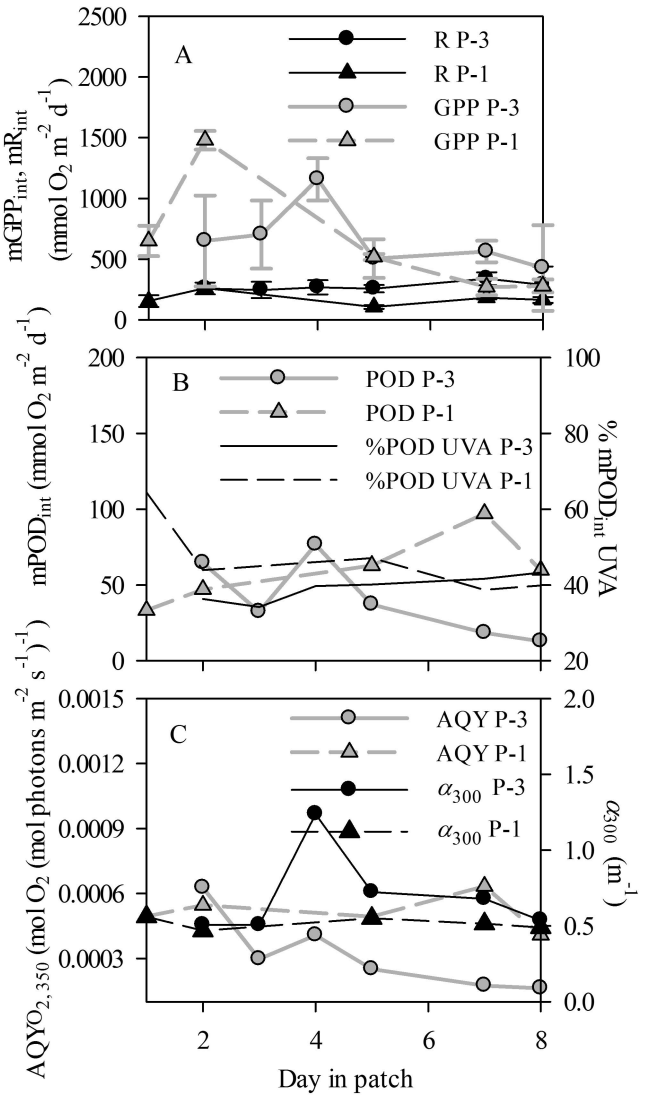

Fig. 5. Model results for (A) euphotic-layer depth-integrated GPP ($mGPP_{int}$) and R (mR_{int}) during Lagrangian expts P-1 and P-3, (B) POD ($mPOD_{int}$) and the percentage of POD accounted for by UVA radiation (%$mPOD_{int}$ UVA), and (C) $AQYO_2$ at 300 nm and CDOM absorbance (α_{300}). Error bars for $mGPP_{int}$ and mR_{int} are based on depth-integrated mean absolute residuals of model output vs. measurements for individual profiles (e.g., Fig. 4).

the majority of our samples were dominated by CDOM and DOC with molecular weights lower than 1 kDa. The absorption spectra of the three samples where high molecular weight appeared to be dominant were characterized by an absorbance shoulder centered around 290–320 nm and typically associated with MAA (Tilstone et al. 2010; Fig. 2). Such a shoulder leads to shallower $S_{275–295}$ and therefore a lower corresponding S_R value.

During this study we carried out irradiations under a constant, simulated light field rather than ambient sunlight. This approach offers distinct advantages by removing both spectral variability and differences in light intensity between experiments that may arise due to cloud cover or the presence of aerosols in the atmosphere. In turn, this facilitates interpretation of the data. It also allowed us to calculate the AQY for O_2 photolysis which may be used to model in situ photochemical O_2 consumption in both space and time, thereby extending the utility of our data beyond the study area, season, and prevalent conditions at the time of sampling. Nevertheless, it is important to highlight some clear uncertainties related to our photochemical work: (1) The spectral resolution of oxygen photolysis in our incubations was limited to two treatments due to logistical constraints. Monochromatic or polychromatic irradiations with 4–6 treatments would have undoubtedly been preferable for the estimation of AQY parameters. Higher spectral resolution would have reduced the uncertainty of the calculated AQY parameters and allowed us to test a linear model of AQY vs. wavelength. (2) All of our samples originated from a depth of 2 m, which limits our understanding of vertical variability in AQY. On the other hand, aquatic photochemical reactions are generally restricted to the upper 10–30 m of the water column, which were found to be relatively homogeneous with regard to temperature, salinity, Chl *a* distribution, and biogeo-

chemical processes such as GPP and R (e.g., Fig. 4). We therefore believe that our AQY data were representative of the surface mixed layer and used these to parameterize a simple one-dimensional photochemical box model.

Our model results show that surface mPOD rates, scaled for ambient irradiance, were in the range of 3.0–15.7 μmol O_2 L^{-1} d^{-1}. These rates were higher than those reported by a previous study in the subtropical Atlantic (0.9–2.8 μmol O_2 L^{-1} d^{-1}; Obernosterer et al. 2001) and lower than in the Amazon River ($\sim$ 40 μmol O_2 L^{-1} d^{-1}; Amon and Benner 1996). These differences presumably reflect differences in the concentration of DOM and CDOM absorbance. The correlation between full-spectrum POD rates and CDOM absorbance at 300 nm (α_{300}; $p < 0.05$) shows that CDOM plays a central role in photochemical oxygen consumption. Furthermore, and in agreement with Andrews et al. (2000), this relationship implies first-order reaction kinetics for POD with respect to CDOM. Surface POD rates would therefore be expected to reflect the distribution of CDOM—lower and higher CDOM absorbance would be expected in the subtropical Atlantic and Amazon River, respectively.

Our polychromatic irradiations showed that the visible range of the spectrum accounted for 20% of the total O_2 photolysis rate in our incubators. We used the respective rates under two polychromatic treatments to formulate the AQY for O_2 photolysis based on the assumption that this is best described by an exponential decrease with increasing wavelength. Andrews et al. (2000) carried out monochromatic irradiations for a variety of mainly inland and coastal waters and found that the wavelength dependence of their data was best described by a linear fit. These authors also parameterized their data with an exponential fit, similar to that described here, which yielded similar results for depth-integrated POD estimates. In the absence of spectrally resolved rates, we were unable to test if a linear model would be more appropriate for our data. However, there are strong reasons to support the assumptions that the AQY for O_2 photolysis follows an exponential decrease with increasing wavelength. The data reported by Andrews et al. (2000) were not corrected for "self-shading." In colored solutions CDOM nearer the source of irradiance may be shading CDOM behind it in the light path. A correction may be applied where self-shading is proportional to CDOM absorbance and the pathlength of the irradiation cell (i.e., the more CDOM absorbance or the longer the pathlength, the higher the effect of self-shading; Zepp 1982). Applying such a spectrally resolved correction to the data reported by Andrews et al. (2000) would have the effect of increasing the AQY in the UV disproportionately to the visible, so that the AQY may be best described by an exponential rather than a linear function. Exponentially decreasing AQY spectra with increasing wavelength have been demonstrated for a variety of aquatic photochemical reactions involving CDOM, including photoproduction of CO (Zafiriou et al. 2003) and CO_2 (Johannessen and Miller 2001). We therefore believe that the exponential formulation employed here does not contradict previous findings, although this clearly needs to be verified through monochromatic irradiations of optically thin solutions.

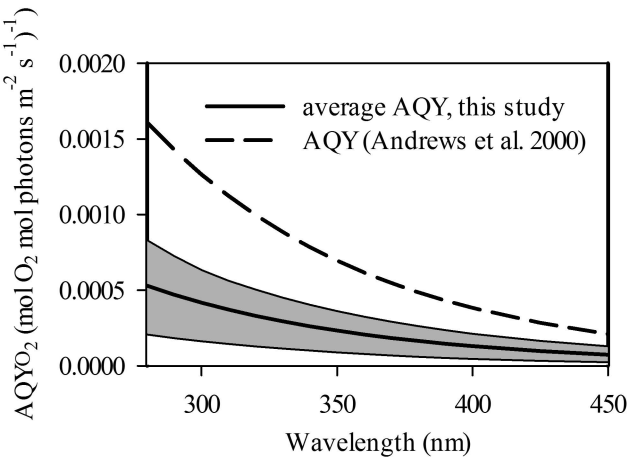

Fig. 6. Average $AQYO_2$ from the present study and the study by Andrews et al. (2000) for Shark River water diluted 1 : 5 with oligotrophic seawater. The shaded area represents minimum and maximum AQY spectra for our experiments.

Our AQY data for O_2 photolysis (0.9–3.6 $\times$ 10^{-4} mol O_2 [mole photons m^{-2} s^{-1}]$^{-1}$ at 350 nm; Table 2) were one order of magnitude lower than those reported by Andrews et al. (2000) for Shark River water (Fig. 6) diluted 1 : 5 with oligotrophic seawater (8–14 $\times$ 10^{-4} mol O_2 [mole photons m^{-2} s^{-1}]$^{-1}$). It should be noted that the difference between the two AQY data sets (Andrews et al. [2000] vs. our data) is likely underestimated because of self-shading effects in the irradiation cell employed in the previous study, i.e., CDOM near the front of the cell was shading CDOM behind it (Andrews et al. 2000). Nevertheless, the average slope of our exponential fit was 0.012 nm^{-1} (range: 0.010–0.016 nm^{-1}), which was identical to the average S_{AQY} given by Andrews et al. (2000) for a 1 : 5 dilution of Shark River water with oligotrophic seawater. This was despite the relatively large errors calculated for S_{AQY} here (Table 2). There are a number of possible explanations that may contribute to the discrepancy in the magnitude of the two AQY data sets. (1) This is unlikely to be due to the respective difference in CDOM absorbance between the two studies (CDOM absorption coefficients were one order of magnitude lower in our study), since normalization by CDOM absorbance is implicit in the calculation of AQY. (2) It is possible that the observed differences in the magnitude of AQY between the present study and that by Andrews et al. (2000) were due to changes in AQY with cumulative absorbed light over time. Andrews et al. (2000) showed that the AQY decreased with increasing absorbed light intensity as CDOM photobleaching proceeded. However, absorbed light intensity was comparable between the two studies, with average absorbed light intensity at 310 nm of 1.3 $\pm$ 0.1 mmol photons m^{-2} s^{-1} L^{-1} here and 0.1–5.5 mmol photons m^{-2} s^{-1} L^{-1} in Andrews et al. (2000). It is therefore unlikely that the respective differences in AQY data are due to differences in absorbed light dose. It should be noted that the absorbed light dose for our experiments represents an upper estimate since it was calculated on the initial CDOM absorbance and did not account for its photobleaching. (3) Most likely the

difference in the magnitude of AQY between our study and that of Andrews et al. (2000) reflects differences in photoreactivity between our respective samples. This may be due to inherent DOM properties (molecular composition) or other factors that are known to affect photoreactivity, such as pH or dissolved Fe (Gao and Zepp 1998).

POD in an upwelling filament—The Mauritanian upwelling is one of the most productive regions in the North Atlantic (Bory et al. 2001). Coastal upwelling transports nutrients into the euphotic zone where they drive phytoplankton growth and ecosystem productivity. Upwelled waters are transported westward to the open ocean in highly dynamic filaments, thus extending the region of high productivity and carbon export into deeper waters. Primary production was therefore highest near the coast and decreased westwards as the upwelled filament moved offshore. Our net community production rates integrated over the euphotic layer (NCP_{int}: 132 ± 48 to 1328 ± 95 mmol O_2 m^{-2} d^{-1}) are among the highest reported rates for the North Atlantic. Previous studies near the western end of our study area reported net autotrophy with NCP_{int} in the region of 50–100 mmol O_2 m^{-2} d^{-1} (Serret et al. 2001; Gist et al. 2009). The Lagrangian nature of our study allowed us to track changes in the biogeochemistry of the upwelled filaments P-1 and P-3. During P-3, a maximum in NCP_{int} (and $mNCP_{int}$) was spatiotemporally associated with a CDOM absorbance maximum (α_{300}; Fig. 5). It is likely that the latter represented newly produced CDOM from biological activity in the upwelling filament. The absorbance spectrum of this ''new CDOM'' was characterized by a clear MAA-like shoulder (Tilstone et al. 2010) and higher AQY values than measured on the previous and following days. In turn, these led to increased POD rates over the euphotic zone. The rapid rise and decline of GPP, CDOM absorbance, AQY, and $mPOD_{int}$ over the following 2 d highlights the transient nature of this event. Alternatively, the CDOM absorbance maximum could be attributed to inputs from deep water. However, we consider this unlikely for the following reasons: (1) The absorbance recorded during this event was higher than in deep waters surveyed during the same cruise (G. Tilstone unpubl. data), (2) the MAA-like absorbance spectrum was not encountered in deep waters, and (3) the spatiotemporal coincidence of the CDOM maximum and NCP strongly suggested a surface source.

POD was a substantial sink for O_2 during both Lagrangian experiments, accounting for 4–59% of R and 3–36% of GPP in the euphotic layer. Obernosterer et al. (2001) found that POD rates in surface waters were consistently and up to 8-fold higher than microbial respiration. Our surface POD rates were also in the same order of magnitude or higher than corresponding respiration rates (3.7–7.4 μmol O_2 L^{-1} d^{-1}). Photochemical reactions in upwelling systems are potentially influenced by high nitrate (NO_3^-, a known photosensitizer). However, POD rates were not related to NO_3^- concentration during our study. NO_3^- remained relatively invariable during each Lagrangian experiment. In contrast to Obernosterer et al. (2001), who found that most of the surface POD was accounted for by visible wavelengths during on-deck incubations (70–100%), we found that UVA radiation accounted for a much larger fraction (66–74%) while UVB accounted for < 5%. However, integrated over the euphotic zone, the contribution by UVB was still found to be negligible, while UVA accounted for a smaller fraction of the total (36–47%, excluding Day 1 of P-1: 65%). Visible radiation therefore dominated the overall POD in the water column. Relatively high AQY values in the UV generally increase the relative importance of this spectral region in surface waters. On the other hand, concomitant high UV light attenuation and low surface incident irradiance in the UV decrease its contribution in the water column. Ultimately, the spectral region that is most important for water column photochemistry is determined by the relative interplay between these factors. Photochemical O_2 activation may contribute to photoinhibition of photosynthesis at the surface through the production of short-lived, highly ROS (hydroxyl, $^{\cdot}OH$; singlet oxygen, $^1O_2$; and superoxide ion, O_2^- radicals) as well as longer-lived hydrogen peroxide (H_2O_2). Our AQY data show that visible radiation may still account for a substantial amount of POD and presumably production of ROS under UV-opaque filter screens used for the determination of NCP. This may explain why GPP was often lower at the surface (~ 2 m) than at 5–8 m irradiance (despite equal or higher Chl *a* concentration), both here and in previous studies (Robinson et al. 2009). Nevertheless, this observation may also be explained by intracellular photoinhibition of photosynthesis, e.g., due to protein damage. The inhibition of GPP by ROS may also explain why in vitro incubations generally yield lower estimates of NCP than geochemical methods. Some degree of depth integration is implicit in the latter, where a surface (typically from 2–7 m on a ship) measurement of O_2 concentration, O_2 : Ar, or O_2 isotopic composition gives an integrated measure of photosynthetic activity over the surface mixed layer of the water column. It is therefore conceivable that primary producers in this layer, which may be transported freely by wave-induced turbulence between the 97% and 55% light depths (2 m and 5–8 m, respectively), are either exposed to a smaller cumulative dose of ROS or allowed sufficient time for repair between periods of high exposure. In contrast, in vitro incubations, by design, remove the effect of variable exposure, thereby resulting in greater cumulative photoinhibition at high light levels. Nevertheless, this point remains speculative in the absence of further data.

Implications for NCP estimates—Current oxygen-based methods for the determination of NCP (in vitro and geochemical methods) do not account for the photochemical O_2 sink. Our work clearly demonstrates that this is a substantial sink, often in the same order of magnitude as respiration. Consequently, NCP is underestimated by all O_2-based methods. In vitro studies, where samples are incubated under UV-opaque filter screens, do not account for POD in the visible range of the spectrum. In our study, the latter contributed 37–65% of total POD (mean and

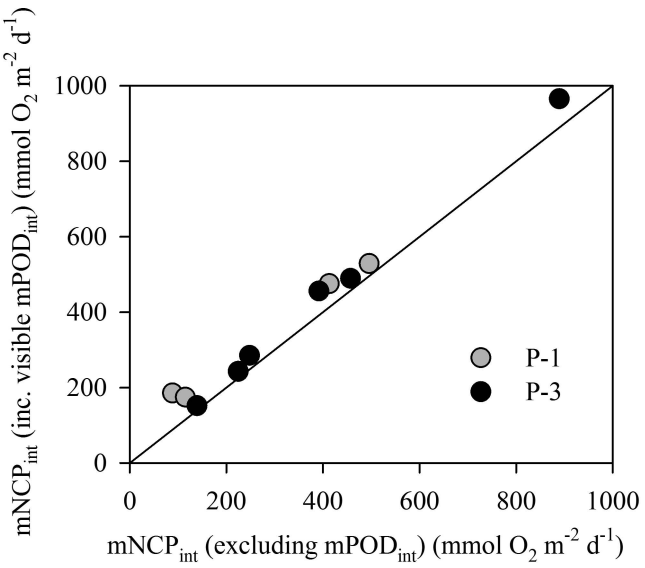

Fig. 7. Net community production based on incubations (NCP excluding POD) vs. NCP accounting for visible O_2 photolysis in borosilicate glass bottles. The solid line represents a 1 : 1 relationship.

standard deviation: 56% ± 8%) in the euphotic zone of the Mauritanian upwelling. NCP was therefore underestimated by 2–46% (mean and standard deviation: 11% ± 14%) during our in vitro incubations. Figure 7 shows that NCP corrected for POD in the visible was consistently higher than NCP excluding POD. These two estimates were strongly correlated (Spearman $R^2 = 0.997$, $p < 0.0001$, $n = 10$), with a slope of 1.0066 ± 0.0244 and intercept of 46.51 ± 13.15 mmol O_2 m^{-2} d^{-1}. Importantly, our data suggest that the relative importance of POD is highest as NCP approaches zero, i.e., balance between autotrophy and heterotrophy. This trophic status describes most of the oligotrophic open ocean. Oxygen-based NCP estimates from in vitro incubations such as our own should therefore be revised upwards in high-productivity waters, such as the Mauritanian upwelling. Further data are required to assess the validity of this relationship in mesotrophic and oligotrophic waters.

The underestimation of NCP calculated through geochemical methods is likely to be even higher, given that these do not account for POD in the UV, which is excluded from in vitro studies by the UV-opaque filter screens. A number of studies have used high-frequency (every 30–60 min) O_2 profiles in the euphotic layer to estimate in situ metabolic rates in aquatic ecosystems (Sambrotto and Langdon 1994). Other studies have examined monthly changes in O_2 profiles to estimate seasonal and interannual NCP variability from long time-series (Cianca et al. 2013). While estimates of R during nighttime would be unaffected by POD in this "open water" method, apparent NCP would be underestimated during daytime, particularly in shallow, clear ecosystems. Similarly, studies measuring O_2 : Ar concentration ratios in seawater (Kaiser et al. 2005) may underestimate NCP as photochemical reactions would consume O_2, but presumably not Ar. Finally, the triple-oxygen-isotope method relies on the principle of mass-dependent O_2 fractionation during photosynthesis and respiration (Kroopnick 1980; Luz and Barkan 2000). To our knowledge, there is only one study that has reported isotopic fractionation during O_2 photolysis in lake water (Chomicki and Schiff 2008). These authors found similar $^{18}O_2 : ^{16}O_2$ fractionation from both respiration and photochemical O_2 consumption. O_2 photolysis would therefore also affect NCP estimates through the triple-isotope approach. To conclude, both in vitro and geochemical methods based on oxygen underestimate NCP in these highly productive waters. Although NCP was not calculated by any geochemical methods here, total POD (UV+visible) accounted for an average of 19% ± 23% of in vitro NCP.

Further studies are needed in order to examine if the relationship shown in Fig. 7 may be extended to less productive, open ocean as well as coastal waters. Photochemical reactions in both coastal and open-ocean waters are likely to be a substantial sink for O_2. In coastal waters, relatively higher CDOM absorbance would be expected to enhance photochemical reactions due to the first-order dependence of POD rates on CDOM. On the other hand, higher light attenuation, particularly in the UV, would be expected to moderate this effect. The roles of CDOM absorbance and light attenuation would be reversed in clear, open-ocean waters where CDOM absorbance is low, but UV penetrates deeper. The hypothesis that this unaccounted O_2 sink may explain the apparent widespread heterotrophy in oligotrophic open-ocean waters remains to be explored.

Acknowledgments

We thank the officers and crew of Royal Research Ship *Discovery* for ensuring the safety and success of our work. We also acknowledge Glen Tarran for flow cytometry data and two anonymous reviewers for the thorough and constructive comments. This work was funded by the UK Natural Environment Research Council through the UK Surface Ocean Lower Atmosphere Study (grant NE/C517176/1), the Oceans 2025 programme, and the Spanish Ministerio de Ciencia e Innovación (grant CTM2008-02037-E). We acknowledge the NERC EO Data Acquisition Service (NEODASS) for near-real time guidance of the research cruise.

References

Amon, R. M. W., and R. Benner. 1996. Photochemical and microbial consumption of dissolved organic carbon and dissolved oxygen in the Amazon River system. Geochim. Cosmochim. Acta **60:** 1783–1792, doi:10.1016/0016-7037(96)00055-5

Andrews, S. S., S. Caron, and O. C. Zafiriou. 2000. Photochemical oxygen consumption in marine waters: A major sink for colored dissolved organic matter? Limnol. Oceanogr. **45:** 267–277, doi:10.4319/lo.2000.45.2.0267

Benson, B. B., and D. Krause. 1984. The concentration and isotopic fractionation of oxygen dissolved in fresh-water and seawater in equilibrium with the atmosphere. Limnol. Oceanogr. **29:** 620–632, doi:10.4319/lo.1984.29.3.0620

Bird, R. E., and R. L. Hulstrom. 1981. A simplified clear sky model for direct and diffuse insolation on horizontal surfaces [Internet]. Golden, Colorado: SERI Technical Report Solar Energy Research Institute [accessed 01 October 2013]. SERI/TR-642-761. Available from http://www.nrel.gov/rredc/pdfs/761.pdf

Bopp, L., and others. 2001. Potential impact of climate change on marine export production. Global Biogeochem. Cycles **15:** 81–99, doi:10.1029/1999GB001256

Bory, A., and others. 2001. Downward particle fluxes within different productivity regimes off the Mauritanian upwelling zone (EUMELI program). Deep-Sea Res. I **48:** 2251–2282, doi:10.1016/S0967-0637(01)00010-3

Bushaw, K. L., and others. 1996. Photochemical release of biologically available nitrogen from aquatic dissolved organic matter. Nature **381:** 404–407, doi:10.1038/381404a0

Carritt, D. E., and J. H. Carpenter. 1966. Comparison and evaluation of currently employed modifications of the Winkler method for determining dissolved oxygen in seawater; a NASCO Report. J. Mar. Res. **24:** 286–319.

Chomicki, K. M., and S. L. Schiff. 2008. Stable oxygen isotopic fractionation during photolytic O-2 consumption in stream waters. Sci. Total Environ. **404:** 236–244, doi:10.1016/j.scitotenv.2008.04.024

Cianca, A., and others. 2013. Oxygen dynamics in the North Atlantic subtropical gyre. Deep-Sea Res. II **93:** 135–147, doi:10.1016/j.dsr2.2013.01.004

Gao, H., and R. G. Zepp. 1998. Factors influencing photoreactions of dissolved organic matter in a coastal river of the southeastern United States. Environ. Sci. Technol. **32:** 2940–2946, doi:10.1021/es9803660

Garcia, H. E., and L. I. Gordon. 1992. Oxygen solubility in seawater—better fitting equations. Limnol. Oceanogr. **37:** 1307–1312, doi:10.4319/lo.1992.37.6.1307

Gist, N., P. Serret, E. M. S. Woodward, K. Chamberlain, and C. Robinson. 2009. Seasonal and spatial variability in plankton production and respiration in the subtropical gyres of the Atlantic Ocean. Deep-Sea Res. II **56:** 931–940, doi:10.1016/j.dsr2.2008.10.035

Hansell, D. A., and C. A. Carlson. 1998. Marine dissolved organic matter and the carbon cycle. Oceanography **14:** 41–49, doi:10.5670/oceanog.2001.05

Helms, J. R., A. Stubbins, J. D. Ritchie, E. C. Minor, D. J. Kieber, and K. Mopper. 2008. Absorption spectral slopes and slope ratios as indicators of molecular weight, source, and photobleaching of chromophoric dissolved organic matter. Limnol. Oceanogr. **53:** 955–969, doi:10.4319/lo.2008.53.3.0955

Johannessen, S. C., and W. L. Miller. 2001. Quantum yield for the photochemical production of dissolved inorganic carbon in seawater. Mar. Chem. **76:** 271–283, doi:10.1016/S0304-4203(01)00067-6

Kaiser, E., and B. Sulzberger. 2004. Phototransformation of riverine dissolved organic matter (DOM) in the presence of abundant iron: Effect on DOM bioavailability. Limnol. Oceanogr. **49:** 540–554, doi:10.4319/lo.2004.49.2.0540

Kaiser, J., M. K. Reuer, B. Barnett, and M. L. Bender. 2005. Marine productivity estimates from continuous O-2/Ar ratio measurements by membrane inlet mass spectrometry. Geophys. Res. Lett **32:** L19605, doi:10.1029/2005GL023459

Kieber, D. J., J. Mcdaniel, and K. Mopper. 1989. Photochemical source of biological substrates in sea water: Implications for carbon cycling. Nature **341:** 637–639, doi:10.1038/341637a0

Kitidis, V., A. P. Stubbins, G. Uher, R. C. Upstill-Goddard, C. S. Law, and E. M. S. Woodward. 2006*a*. Variability of chromophoric organic matter in surface waters of the Atlantic Ocean. Deep-Sea Res. II **53:** 1666–1684, doi:10.1016/j.dsr2.2006.05.009

———, G. Tilstone, T. Smyth, R. Torres, and C. S. Law. 2011. Carbon monoxide emission from a Mauritanian upwelling filament. Mar. Chem. **127:** 123–133, doi:10.1016/j.marchem.2011.08.004

———, G. Uher, R. C. Upstill-Goddard, R. F. C. Mantoura, G. Spyres, and E. M. S. Woodward. 2006*b*. Photochemical production of ammonium in the oligotrophic Cyprus Gyre (Eastern Mediterranean). Biogeosciences **3:** 439–449, doi:10.5194/bg-3-439-2006

Kroopnick, P. 1980. Isotopic fractionations during oxygen-consumption and carbonate dissolution within the North-Atlantic deep-water. Earth Planet. Sci. Lett. **49:** 485–498.

Laane, R., W. W. C. Gieskes, G. W. Kraay, and A. Eversdijk. 1985. Oxygen-consumption from natural-waters by photo-oxidizing processes. Neth. J. Sea Res. **19:** 125–128, doi:10.1016/0077-7579(85)90016-X

Luz, B., and E. Barkan. 2000. Assessment of oceanic productivity with the triple-isotope composition of dissolved oxygen. Science **288:** 2028–2031, doi:10.1126/science.288.5473.2028

McCarthy, M. D., J. I. Hedges, and R. Benner. 1998. Major bacterial contribution to marine dissolved organic nitrogen. Science **281:** 231–234, doi:10.1126/science.281.5374.231

Micinski, E., L. A. Ball, and O. C. Zafiriou. 1993. Photochemical oxygen activation—superoxide radical detection and production-rates in the eastern Caribbean. J. Geophys. Res.: Oceans **98:** 2299–2306, doi:10.1029/92JC02766

Miller, W. L., M. A. Moran, W. M. Sheldon, R. G. Zepp, and S. Opsahl. 2002. Determination of apparent quantum yield spectra for the formation of biologically labile photoproducts. Limnol. Oceanogr. **47:** 343–352, doi:10.4319/lo.2002.47.2.0343

———, and R. G. Zepp. 1995. Photochemical production of dissolved inorganic carbon from terrestrial organic-matter—significance to the oceanic organic-carbon cycle. Geophys. Res. Lett. **22:** 417–420, doi:10.1029/94GL03344

Mopper, K., X. L. Zhou, R. J. Kieber, D. J. Kieber, R. J. Sikorski, and R. D. Jones. 1991. Photochemical degradation of dissolved organic-carbon and its impact on the oceanic carbon-cycle. Nature **353:** 60–62, doi:10.1038/353060a0

Moran, M. A., W. M. Sheldon, and R. G. Zepp. 2000. Carbon loss and optical property changes during long-term photochemical and biological degradation of estuarine dissolved organic matter. Limnol. Oceanogr. **45:** 1254–1264, doi:10.4319/lo.2000.45.6.1254

Nelson, N. B., D. A. Siegel, and A. F. Michaels. 1998. Seasonal dynamics of colored dissolved material in the Sargasso Sea. Deep-Sea Res. I **45:** 931–957, doi:10.1016/S0967-0637(97)00106-4

O'Sullivan, D. W., P. J. Neale, R. B. Coffin, T. J. Boyd, and S. L. Osburn. 2005. Photochemical production of hydrogen peroxide and methylhydroperoxide in coastal waters. Mar. Chem. **97:** 14–33, doi:10.1016/j.marchem.2005.04.003

Obernosterer, I., and G. J. Herndl. 2000. Differences in the optical and biological reactivity of the humic and non-humic dissolved organic carbon component in two contrasting coastal marine environments. Limnol. Oceanogr. **45:** 1120–1129, doi:10.4319/lo.2000.45.5.1120

———, P. Ruardij, and G. J. Herndl. 2001. Spatial and diurnal dynamics of dissolved organic matter (DOM) fluorescence and H_2O_2 and the photochemical oxygen demand of surface water DOM across the subtropical Atlantic Ocean. Limnol. Oceanogr. **46:** 632–643, doi:10.4319/lo.2001.46.3.0632

Pelletier, G. 2008. A solar position and radiation calculator for Microsoft Excel/VBA [Internet]. Olympia, Washington [accessed 01 October 2013]. Available from http://www.ecy.wa.gov/programs/eap/models.html

Platt, T., C. L. Gallegos, and W. G. Harrison. 1980. Photoinhibition of photosynthesis in natural assemblages of marine-phytoplankton. J. Mar. Res. **38:** 687–701.

Robinson, C., and others. 2009. Comparison of in vitro and in situ plankton production determinations. Aquat. Microb. Ecol. **54:** 13–34, doi:10.3354/ame01250

Rose, A. L., and D. Waite. 2006. Role of superoxide in the photochemical reduction of iron in seawater. Geochim. Cosmochim. Acta **70:** 3869–3882, doi:10.1016/j.gca.2006.06.008

Sambrotto, R. N., and C. Langdon. 1994. Water column dynamics of dissolved inorganic carbon (DIC), nitrogen and O_2 on Georges Bank during April, 1990. Cont. Shelf Res. **14:** 765–789, doi:10.1016/0278-4343(94)90072-8

Scully, N. M., W. J. Cooper, and L. J. Tranvik. 2003. Photochemical effects on microbial activity in natural waters: The interaction of reactive oxygen species and dissolved organic matter. FEMS Microbiol. Ecol. **46:** 353–357, doi:10.1016/S0168-6496(03)00198-3

Serret, P., C. Robinson, E. Fernandez, E. Teira, and G. Tilstone. 2001. Latitudinal variation of the balance between plankton photosynthesis and respiration in the eastern Atlantic Ocean. Limnol. Oceanogr. **46:** 1642–1652, doi:10.4319/lo.2001.46.7.1642

Smyth, T. J. 2011. Penetration of UV irradiance into the global ocean. J. Geophys. Res.: Oceans **116:** C11020, doi:10.1029/2011JC007183

Stedmon, C. A., S. Markager, L. Tranvik, L. Kronberg, T. Slätis, and W. Martinsen. 2007. Photochemical production of ammonium and transformation of dissolved organic matter in the Baltic Sea. Mar. Chem. **104:** 227–240, doi:10.1016/j.marchem.2006.11.005

Steinberg, D. K., N. B. Nelson, C. A. Carlson, and A. C. Prusak. 2004. Production of chromophoric dissolved organic matter (CDOM) in the open ocean by zooplankton and the colonial cyanobacterium *Trichodesmium* spp. Mar. Ecol. Prog. Ser. **267:** 45–56, doi:10.3354/meps267045

Stubbins, A. R., and others. 2010. Illuminated darkness: Molecular signatures of Congo River dissolved organic matter and its photochemical alteration as revealed by ultrahigh precision mass spectrometry. Limnol. Oceanogr. **55:** 1467–1477, doi:10.4319/lo.2010.55.4.1467

Tilstone, G. H., R. L. Airs, V. Martinez-Vicente, C. Widdicombe, and C. A. Llewellyn. 2010. High concentrations of mycosporine-like amino acids and colored dissolved organic matter in the sea surface microlayer off the Iberian Peninsula. Limnol. Oceanogr. **55:** 1835–1850, doi:10.4319/lo.2010.55.5.1835

Vähätalo, A. V., and R. G. Wetzel. 2004. Photochemical and microbial decomposition of chromophoric dissolved organic matter during long (months-years) exposures. Mar. Chem. **89:** 313–326, doi:10.1016/j.marchem.2004.03.010

———, and R. G. Zepp. 2005. Photochemical mineralization of dissolved organic nitrogen to ammonium in the Baltic Sea. Environ. Sci. Technol. **39:** 6985–6992, doi:10.1021/es050142z

Vodacek, A., N. V. Blough, M. D. Degrandpre, E. T. Peltzer, and R. K. Nelson. 1997. Seasonal variation of CDOM and DOC in the Middle Atlantic Bight: Terrestrial inputs and photooxidation. Limnol. Oceanogr. **42:** 674–686, doi:10.4319/lo.1997.42.4.0674

Welshmeyer, N. A. 1994. Fluorometric analysis of chlorophyll *a* in the presence of chlorophyll *b* and phaeopigments. Limnol. Oceanogr. **39:** 1985–1992, doi:10.4319/lo.1994.39.8.1985

Zafiriou, O. C. 1974. Sources and reactions of OH and daughter radicals in seawater. J. Geophys. Res. **79:** 4491–4497, doi:10.1029/JC079i030p04491

———, S. S. Andrews, and W. Wang. 2003. Concordant estimates of oceanic carbon monoxide source and sink processes in the Pacific yield a balanced global "blue-water" CO budget. Global Biogeochem. Cycles **17:** 1015, doi:10.1029/2001GB001638

Zepp, R. G. 1982. Experimental approaches to environmental photochemistry, p. 19–41. *In* O. Hutzinger [ed.], The handbook of environmental chemistry. V. 2 pt. B. Springer Verlag.

———, B. C. Faust, and J. Hoigne. 1992. Hydroxyl radical formation in aqueous reactions (pH 3–8) of Iron(II) with hydrogen peroxide: The photo-fenton reaction. Environ. Sci. Technol. **26:** 313–319, doi:10.1021/es00026a011

———, N. L. Wolfe, G. L. Baughman, and R. C. Hollis. 1977. Singlet oxygen in natural-waters. Nature **267:** 421–423, doi:10.1038/267421a0

Associate editor: Heidi M. Sosik

Received: 07 May 2013
Accepted: 25 October 2013
Amended: 28 October 2013